Polarization Modulated CPT and Population Distributions Among Ground-State Zeeman Sublevels

Zachary Warren, Hunter Kettering, Andrew Householder, and James Camparo
Physical Sciences Laboratories
The Aerospace Corporation
El Segundo, CA, USA

***Summary*—Chip-scale atomic clocks (CSAC) are the products of a burgeoning field of miniature precise timing efforts in support of low-SWaP space-qualified timing sources. Most CSACs are based on the coherent population trapping (CPT) effect, which uses laser light to selectively pump atoms into dark states. Because of the multiple accessible and inaccessible hyperfine Zeeman states, many atoms don't contribute to the signal leading to a low signal-to-noise ratio of the CPT resonance. In turn, clock stability is limited. While solutions to this problem have been studied previously, the examination of the redistribution of atoms through the novel pumping solutions has not been thoroughly studied. This work provides continued exploration of an experimental effort to evaluate Zeeman end-state recovery schemes.**

Keywords—coherent population trapping; multipole moments; atomic clock; polarization; density matrix

I. Introduction

Chip-scale atomic clocks (CSACs) are limited in performance by low signal-to-noise ratio (SNR), a contributor to poor clock performance. Generating the coherent population trapping (CPT) resonance for use in CSACs is typically achieved with a microwave-frequency modulated Vertical Cavity Surface Emitting Laser (VCSEL). Unfortunately, the polarized light employed in the basic CPT scheme leads to atoms shuttled into extreme Zeeman end states, generally known as trap-states. Though recognized as detrimental to CSAC SNRs, with mitigation strategies an important research topic for next-generation CSACs, to date there have been few quantitative studies of population distributions among ground-state Zeeman sublevels during CPT. Though our studies focus on ^{87}Rb as a representative species to evaluate the ground state distributions, the method is applicable to any warm vapor clock resonance.

The Zeeman end-state recovery method we are presently evaluating in our laboratory is phase-and-polarization modulation. In this technique, the laser polarization is modulated at nearly 1 kHz, enabling optical pumping of atoms out of the Zeeman end-states. Due to the deleterious phase changes in the Rabi frequency from the polarization switching, the microwave phase is also modulated to correct this, producing a higher SNR dual-modulation CPT (DM-CPT). In our experiments, we add a collinear test probe laser to the CPT-generating laser and tune the probe across the D_1 absorption profile. The probe spectrum contains information on the population distribution. Other studies have been performed on the distribution of atom populations, though not covering polarization modulation [1,2].

We have reported on this test setup and methodology previously [3-5], utilizing the trap-state recovery method implemented in detail in Yun *et al* (2014) [6,7]. The careful study of ground-state population distributions during clock resonance generation enables the optimization of Zeeman end-state accumulation mitigation strategies for CPT. Our previous work initiated those studies by quantifying ground-state population distributions via three density-matrix multipole moments for the hyperfine levels involved: the monopole η_F, dipole $\langle F_z \rangle$, and quadrupole $\langle Q_F \rangle$ moments [8,9]. A pump-probe experiment to test the impact of CPT on the population distributions unveils the distribution experimentally. The analysis was performed directly on the collected data, which included extraneous noise in the result.

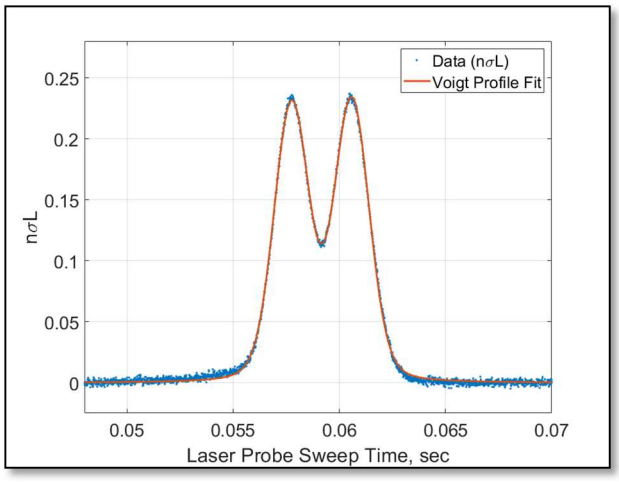

Figure 1: Example of Voigt profile fitting to a representative clean absorption profile in ^{87}Rb over a range of approximately 2 GHz. The two resolved transitions correspond to $5^2S_{1/2}(F_g=2) \rightarrow 5^2P_{1/2}(F_e=1)$ and $5^2S_{1/2}(F_g=2) \rightarrow 5^2P_{1/2}(F_e=2)$.

In this paper we will discuss our latest advance in the ability to assess CPT ground-state population distributions. Briefly, in our previous work we only assessed η_F (the fractional population in a specific ground-state hyperfine level) and $\langle F_z \rangle$ (the orientation of the atom's angular momentum along the quantization axis). To determine $\langle Q_F \rangle$ (the alignment of angular momentum along the quantization axis) requires an analysis of

the separate transitions from one ground-state hyperfine level to one excited-state hyperfine level, and in our previous work we had not yet included this in our analysis.

To determine η_F, $\langle F_z \rangle$ *and* $\langle Q_F \rangle$ we now fit a Voigt profile to the overlapped resonances as illustrated in the representative Fig. 1. From the fit we can determine the strength of each transition separately to the overall lineshape, and, from that information extract all three parameters describing the ground-state population distribution. Together, the monopole moment, dipole moment, and quadrupole moment are the maximum amount of information one can extract regarding ground-state population distribution using 1-photon dipole transitions.*

In what follows we demonstrate Voigt profile fitting as a means to more accurately extract absorption profile information and disentangle the two overlapped excited-state hyperfine transitions. Quadrupole moment information is now accessible with this method, providing a major improvement over our previous efforts.

II. METHODS

The CPT clock signal is formed via specific optical transitions and atoms are accumulated in the Zeeman end states (*e.g.* $m_F = +2$) through excitation and spontaneous emission. This effect limits the population available to the CPT transition and reduces the signal amplitude. The end states are not coupled to excited states for this optical polarization and selection rule configuration (*e.g.* $\sigma^{\pm} \rightarrow m_{F'} = m_F \pm 1$), shown in Fig. 2 (left).

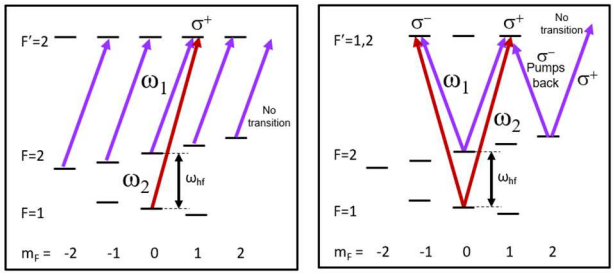

Figure 2: CPT pumping schemes utilizing single polarization on the left and polarization modulation on the right

Alternating the selection rules via polarization modulation, Fig. 2 (right), results in a redistribution of the ground state populations. This method simultaneously produces a CPT doublet despite a reintroduction of the atom population into the system – the two Λ systems do not constructively add [6]. As in previous studies, through evaluation of the population distribution via state multipole analysis, we can validate and optimize diverse Zeeman end-state recovery methods for overall improvement of CSAC designs.

To measure the state multipoles in CPT, we use a distributed feedback (DFB) laser and a VCSEL to launch light through a vapor cell containing ^{87}Rb, shown in Fig. 3. The DFB probe laser was attenuated to 20 nW of total optical power to eliminate any potential of optical pumping and chopped for detection separate from the pump via a lock-in amplifier. Each laser has independent adjustable polarizations for the range of tests we perform. The modulated VCSEL generates CPT, while the single frequency DFB laser is tuned over the rubidium absorption spectrum. The beamsplitter after the chopper is used for a second path of probe monitoring.

Our previous method of probe-spectra analysis yielded the monopole moment of the population distribution and the dipole moment of the population distribution. We did not determine the quadrupole moment of the population distribution, since this requires analysis of the individual excited state hyperfine transitions. Nevertheless, many of the details involved in the calculation are reported in our publications [3-5]. The final step of analysis discussed here involves Voigt-fitting the complete absorption spectrum, determining the population distributions from those measurements, and from those population-distribution multipole moments calculating density matrix population values $\rho_{m,m}$ for each of the m_F Zeeman ground state sublevels.†

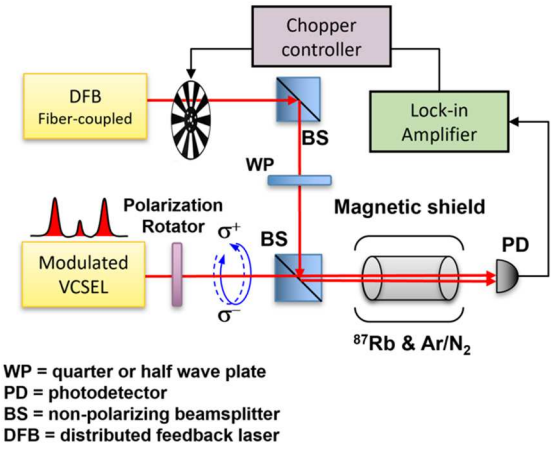

Figure 3: The test setup uses a microwave-modulated VCSEL to prepare CPT, while a DFB probe tunes over the optical resonances and is optically chopped for lock-in detection; the polarization rotator is used for generating alternative CPT schemes.

III. RESULTS AND DISCUSSION

Using the testbed, Figs. 4 and 5 are measurements of the absorption with the probe laser sweeping across the rubidium spectrum collected via lock-in detection during CPT operation with the modulated VCSEL. During CPT operation, the atoms in state **a** become depleted, having contributed to CPT and shuttling to the end state from which there is no transition.

* For a 1-photon dipole transition the absorption spectrum is determined by $|\langle e|\mathbf{r}|g\rangle|^2$, where **r** is a vector operator. Thus, if we imagine **r** is as an L = 1 spherical harmonic, then since the absorption probability scales like $\mathbf{r}^2$, a 1-photon absorption spectrum only carries information on population distributions described by angular momenta J = 2,1,0: quadrupole, dipole and monopole population distributions.

† Since we only determine three state multipole moments (i.e., η_F, $\langle F_z \rangle$ and $\langle Q_F \rangle$), we can only *estimate* the population distribution in the $F_g = 2$ hyperfine level, which has five Zeeman sublevels; we essentially assume that the octupole and hexadecapole multipole moments are zero. However, for $F_g = 1$ with three Zeeman sublevels our determination of the population in these sublevels is exact.

Subsequently when more circularly polarized light arrives, there are fewer atoms to absorb that light, so the resonances remain low. In contrast, during DM-CPT operation, more atoms are involved at all times as those ending up in the Zeeman end state are returned to the system enabling more absorption.

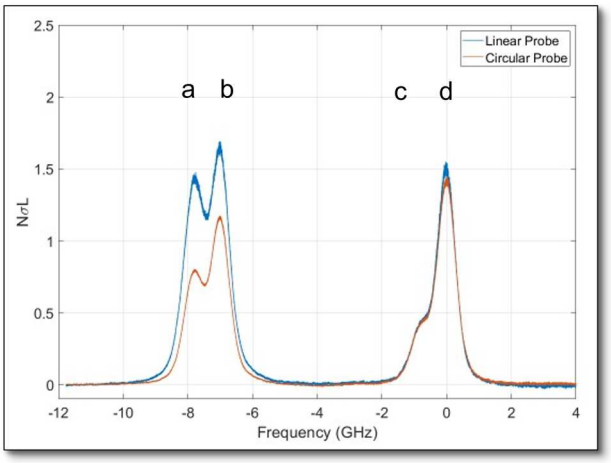

Figure 4: Measurement of the hyperfine transitions via this pump-probe method where the pump laser is in the traditional CPT mode (i.e., circularly polarized). The darker color (or blue) indicates a linearly polarized probe, while the lighter color (or orange) indicates a circularly polarized probe. The transitions **a** to **d** correspond to: $5^2S_{1/2}(F_g=2) \rightarrow 5^2P_{1/2}(F_e=1)$, $5^2S_{1/2}(F_g=2) \rightarrow 5^2P_{1/2}(F_e=2)$, $5^2S_{1/2}(F_g=1) \rightarrow 5^2P_{1/2}(F_e=1)$ and $5^2S_{1/2}(F_g=1) \rightarrow 5^2P_{1/2}(F_e=2)$, respectively.

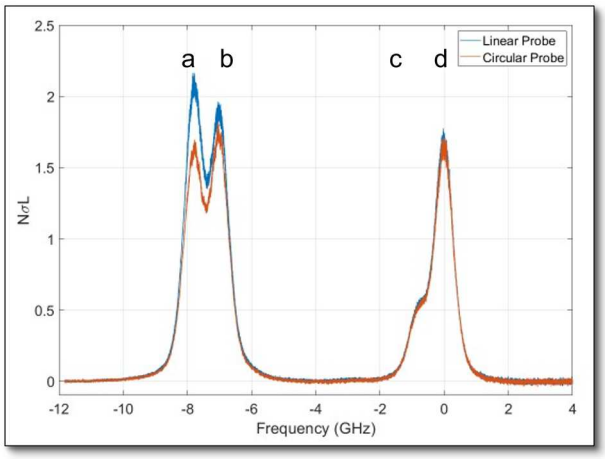

Figure 5: Measurement of the hyperfine transitions via this pump-probe method where the pump laser is in the DM-CPT mode. The darker color (or blue) indicates a linearly polarized probe while the lighter color (or orange) indicates a circularly polarized probe.

In Figs. 6 and 7 we demonstrate the individual fitting of the hyperfine transitions and how they combine to form the entire spectrum. Fitting a Voigt profile to individual hyperfine transitions enables determination of 1) the fractional population in hyperfine level, 2) $\langle F_z \rangle$, and 3) the degree of angular momentum alignment in each hyperfine level, $\langle Q_F \rangle$. With these three parameters, individual Zeeman sublevel populations can be estimated.

The measurement requires that we collect traces of all the hyperfine transitions with a polarized probe laser during CPT operation of the pump laser for multiple probe intensities. For each probe intensity we fit the spectra to a set of Voigt profile resonances, and from those fits extract values of η_F, $\langle F_z \rangle$ and $\langle Q_F \rangle$ for each ground-state hyperfine level. Plotting those parameters as a function of probe light intensity, we extrapolate to zero probe laser intensity. Extrapolation ensures that our estimates of η_F, $\langle F_z \rangle$ and $\langle Q_F \rangle$ are not confounded by any probe optical pumping.

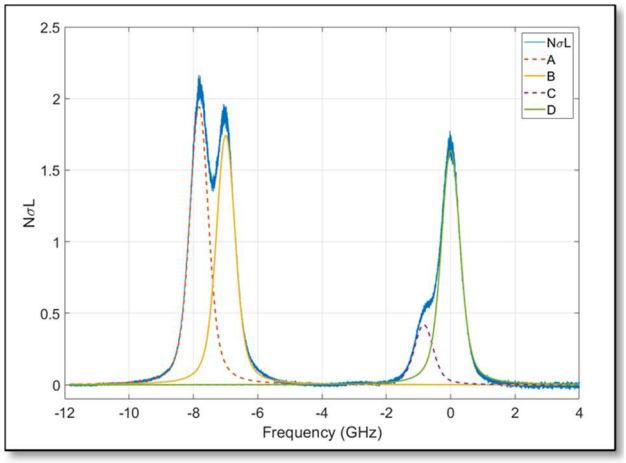

Figure 6: Four Voigt profiles that comprise the four hyperfine transitions

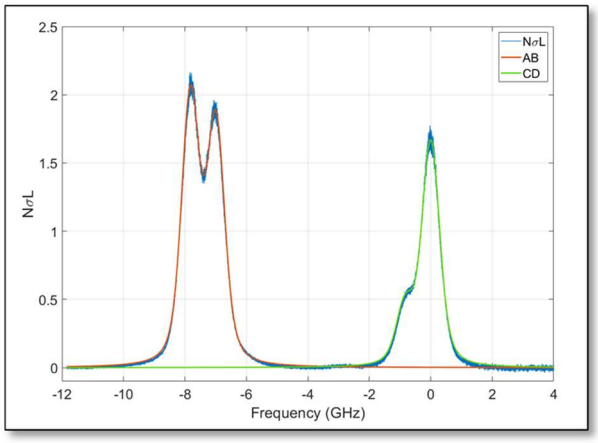

Figure 7: The sum of the Voigt profiles, one sum for each ground state transition, fit the data well.

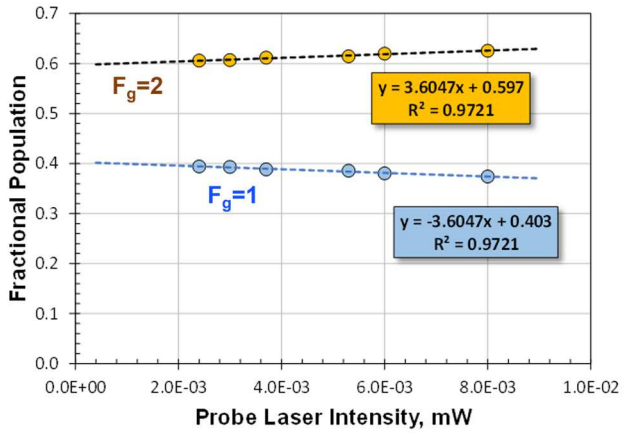

Figure 8: Fractional population as a function of probe laser intensity for the two ground states in ^{87}Rb, enabling extrapolation to zero power for the overall population distribution.

For standard CPT in our experimental system the three graphs in Figs. 8-10 show the dependence of the various population distribution parameters on the probe laser intensity. To extrapolate to zero probe power, we assume a linear dependence, which appears to be consistent with the data. Note that there is considerable scatter in the estimated value of $\langle Q_{F=1} \rangle$. This is due to the fact that the $5^2S_{1/2}(F_g=1) \rightarrow 5^2P_{1/2}(F_e=1)$ transition is relatively small, and it is difficult to estimate its amplitude inside the wing of the (overlapped) $5^2S_{1/2}(F_g=1) \rightarrow 5^2P_{1/2}(F_e=2)$ transition.

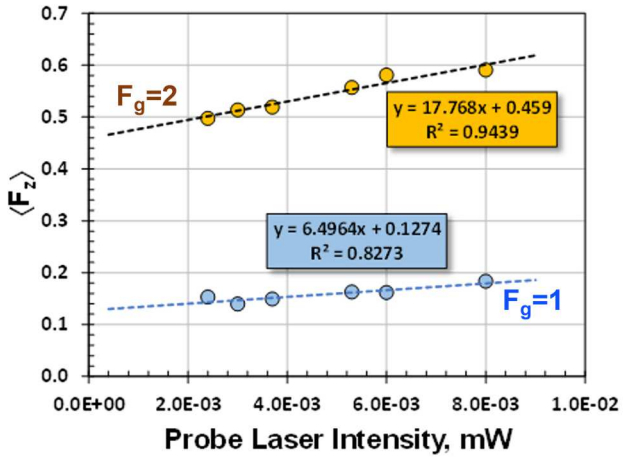

Figure 9: $\langle F_z \rangle$ as a function of probe laser intensity for the two ground states in ^{87}Rb, enabling extrapolation to zero power for the spin polarization states.

‡ If the buffer-gas pressure broadening is large enough, the excited state hyperfine splitting will not be resolved. If the excited state hyperfine splitting is unresolved by the pump laser, then $\langle Q_F \rangle = 0$.

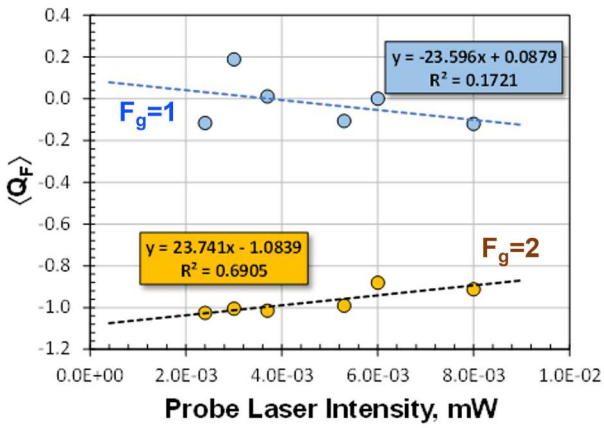

Figure 10: $\langle Q_F \rangle$ as a function of probe laser intensity for the two ground states in ^{87}Rb, enabling extrapolation to zero power for the alignment of the angular momentum states.

From the mean values of the probe laser intercepts and the uncertainties of those intercepts, we were able to determine estimated values of the population in each of the ground-state Zeeman sublevels along with an estimate of the uncertainty in that estimate. The results are shown in Figs. 11 and 12. Note that the non-zero value of the population distribution quadrupole moment (i.e., angular momentum alignment) has a significant effect on the population distributions. In particular, there are two significant aspects to these results:

1. The amount of population in the trapping end state *is less than expected*. In essence, the non-zero value of the quadrupole moment forces atomic population into the $m_F = 0$ state at the expense of the end state.
2. There is an important difference in the population of the two m_F=0 Zeeman sublevels, which affects the magnitude of the spin-exchange shift [10]. Thus, since the degree of this population difference will depend on the laser intensity (via orientation and alignment optical pumping) as well as the buffer-gas pressure (via resolution of the excited hyperfine splitting‡), the spin-exchange shift will take on a laser intensity and buffer-gas pressure dependence.

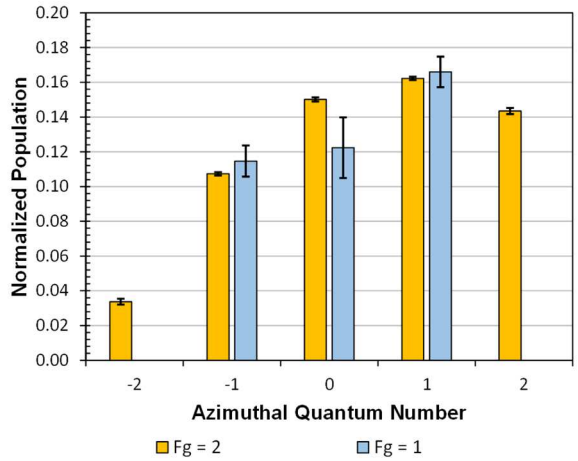

Figure 11: The best estimate of the population distribution is shown here for the two ground-state hyperfine levels, with a Zeeman end-state noticeably smaller than anticipated likely from the quadrupole moment's contribution to the population distribution.

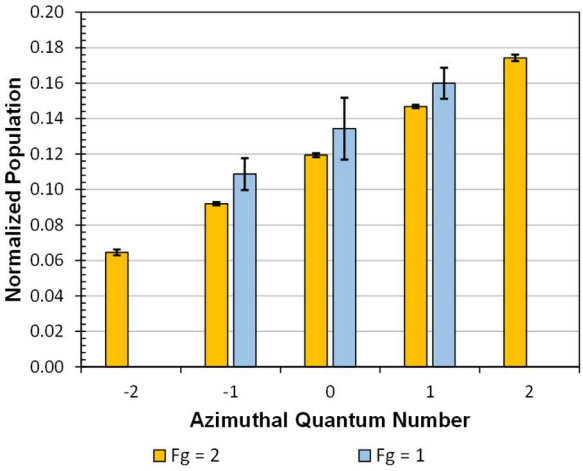

Figure 12: Using the same η_e and $\langle F_e \rangle$ parameters of Fig. 11, but setting $\langle Q_F \rangle = 0$, this figure illustrates the important role of the quadrupole moment on the ground-state population distribution.

IV. Conclusion

Traditional CPT clock performance can be limited by non-contributing atoms in the ground states leading to atomic clocks that can be improved via enhanced SNR. Thus, enhancement methods require further study. Our multipole state analysis can help identify the impacts of Zeeman end-state recovery methods on the complete ground-state population distribution with implications (for example) to a clock's resulting spin-exchange shift. With the present work, our ability to analyze ground-state population distributions based on the monopole moment, dipole moment (i.e., angular momentum polarization) and quadrupole moment (i.e., angular momentum alignment) is complete. Our next steps will aim at examining these population distributions for standard CPT and DM-CPT as functions of pump laser intensity, buffer-gas pressure and vapor temperature.

References

[1] Y. Shi, T. Scholtes, Z. D. Grujić, V. Lebedev, V. Dolgovskiy, and A. Weis, "Quantitative study of optical pumping in the presence of spin-exchange relaxation," Phys. Rev. A 97, 013419 (2018).

[2] J. Xu, G. Wäckerle, and M. Mehring, "Optical detection of spin multipole order in the ground state of alkali atoms," Z Phys D - Atoms, Molecules and Clusters 42, 5–13 (1997).

[3] Z. Warren and J. Camparo, "Measuring Multipole Moments of the CPT Density Matrix Under Optical Field Polarization-Modulation Conditions," Proceedings of the 53rd Annual Precise Time and Time Interval Systems and Applications Meeting, Long Beach, California, January 2022, pp. 80-86.

[4] Z. Warren, J. Camparo, "Measuring multipole moments of the CPT density matrix during optical polarization modulation," Proc. SPIE 12016, Optical and Quantum Sensing and Precision Metrology II, 1201605 (2022).

[5] Z. Warren and J. Camparo, "Multipole Moments of the CPT Density Matrix in Polarization Modulation Conditions," 2022 Joint Conference of the European Frequency and Time Forum and IEEE International Frequency Control Symposium (EFTF/IFCS), pp. 1-4 (2022)

[6] M. Huang and J. C. Camparo, Coherent population trapping under periodic polarization modulation: Appearance of the CPT doublet, Phys. Rev. A 85, 012509 (2012).

[7] P. Yun, J.-M. Danet, D. Holleville, E. de Clercq, and S. Guérandel, "Constructive polarization modulation for coherent populating trapping clock," Appl. Phys. Lett. 105, 231106 (2014).

[8] K. Blum, Density Matrix Theory and Applications (Plenum Press, New York, 1981).

[9] D. Budker, D. F. Kimball, and D. P. DeMille, Atomic Physics (Oxford University Press, Oxford, UK 2.

[10] S. Micalizio, A. Godone, F. Levi, and J. Vanier, "Spin-exchange shift in alkali-metal-vapor cell frequency standards," Phys. Rev. A 70, 033414 (2006).